Optimisation of Amplitude Limiters for Phase Preservation Based on the Exact Solution to Degenerate Four-Wave Mixing

K. R. H. Bottrill,* G. Hesketh, F. Parmigiani, D. J. Richardson and P. Petropoulos

Optoelectronics Research Centre, University of Southampton, Southampton, SO17 1BJ, UK

**krhb1g12@soton.ac.uk*

Abstract: Adopting an exact solution to four-wave mixing (FWM), wherein harmonic evolution is described by the sum of two Bessel functions, we identify two causes of amplitude to phase noise conversion which impair FWM saturation based amplitude regenerators: self-phase modulation (SPM) and Bessel-order mixing (BOM). By increasing the pump to signal power ratio, we may arbitrarily reduce their impact, realising a phase preserving amplitude regenerator. We demonstrate the technique by applying it to the regeneration of a 10 GBaud QPSK signal, achieving a high level of amplitude squeezing with minimal amplitude to phase noise conversion.

OCIS codes: (190.4380) Nonlinear optics, four-wave mixing; (190.4970) Parametric oscillators and amplifiers; (200.6015) Signal regeneration; (060.1155) All-optical networks.

References and links

1. Z. Lali-Dastjerdi, M. Galili, H. C. H. Mulvad, H. Hu, L. K. Oxenløwe, K. Rottwitt, and C. Peucheret, "Parametric amplification and phase preserving amplitude regeneration of a 640 gbit/s rz-dpsk signal," Opt. Express **21**, 25944–25953 (2013).
2. M. Matsumoto and T. Kamio, "Nonlinear phase noise reduction of dqpsk signals by a phase-preserving amplitude limiter using four-wave mixing in fiber," Selected Topics in Quantum Electronics, IEEE Journal of **14**, 610–615 (2008).
3. M. Matsumoto and K. Sanuki, "Performance improvement of dpsk signal transmission by a phase-preserving amplitude limiter," Opt. Express **15**, 8094–8103 (2007).
4. A. Striegler, M. Meissner, K. Cvecek, K. Sponsel, G. Leuchs, and B. Schmauss, "Nolm-based rz-dpsk signal regeneration," Photonics Technology Letters, IEEE **17**, 639–641 (2005).
5. X. Huang, Z. Zhang, C. Qin, Y. Yu, and X. Zhang, "Optimized quantum well semiconductor optical amplifier for rz-dpsk signal regeneration," Quantum Electronics, IEEE Journal of **47**, 819–826 (2011).
6. T. Torounidis, P. Andrekson, and B. Olsson, "Fiber-optical parametric amplifier with 70-db gain," Photonics Technology Letters, IEEE **18**, 1194–1196 (2006).
7. S. Yoo, "Wavelength conversion technologies for wdm network applications," Lightwave Technology, Journal of **14**, 955–966 (1996).
8. P. Minzioni, V. Pusino, I. Cristiani, L. Marazzi, M. Martinelli, C. Langrock, M. M. Fejer, and V. Degiorgio, "Optical phase conjugation in phase-modulated transmission systems: experimental comparison of different nonlinearity-compensation methods," Opt. Express **18**, 18119–18124 (2010).
9. J. Hansryd, P. Andrekson, M. Westlund, J. Li, and P. Hedekvist, "Fiber-based optical parametric amplifiers and their applications," Selected Topics in Quantum Electronics, IEEE Journal of **8**, 506–520 (2002).
10. E. Lichtman, A. A. Friesem, R. G. Waarts, and H. H. Yaffe, "Exact solution of four-wave mixing of copropagating light beams in a kerr medium," J. Opt. Soc. Am. B **4**, 1801–1805 (1987).

11. M. E. Marhic, *Fiber Optical Parametric Amplifiers, Oscillators and Related Devices* (Cambridge University, 2007).
12. M. E. Marhic, K. K. Y. Wong, M. C. Ho, and L. G. Kazovsky, "92% pump depletion in a continuous-wave one-pump fiber optical parametric amplifier," Opt. Lett. **26**, 620–622 (2001).
13. K. Bottrill, G. Hesketh, F. Parmigiani, D. Richardson, and P. Petropoulos, "Investigation into the role of pump to signal power ratio in fwm-based phase preserving amplitude regeneration," in "CLEO: 2015," (Optical Society of America, 2015), p. SM2M.1.
14. L. Gruner-Nielsen, S. Dasgupta, M. Mermelstein, D. Jakobsen, S. Herstrom, M. Pedersen, E. Lim, S. Alam, F. Parmigiani, D. Richardson, and B. Palsdottir, "A silica based highly nonlinear fibre with improved threshold for stimulated brillouin scattering," in "ECOC 2010," (2010), pp. 1–3.
15. Y. Takushima and T. Okoshi, "Suppression of stimulated brillouin scattering using optical isolators," Electronics Letters **28**, 1155–1157 (1992).
16. C. Lundstrom, R. Malik, L. Gruner-Nielsen, B. Corcoran, S. Olsson, M. Karlsson, and P. Andrekson, "Fiber optic parametric amplifier with 10-db net gain without pump dithering," Photonics Technology Letters, IEEE **25**, 234–237 (2013).
17. G. Agrawal, *Nonlinear Fiber Optics, Fifth Edition (Optics and Photonics)* (Academic, 2012).
18. M. Matsumoto, "Phase noise generation in an amplitude limiter using saturation of a fiber-optic parametric amplifier," Opt. Lett. **33**, 1638–1640 (2008).
19. G. Hesketh, K. R. H. Bottrill, F. Parmigiani, D. J. Richardson, and P. Petropoulos, "On the role of signal-pump ratio in fwm-based phase preserving amplitude regeneration," in "International Conference on Optical Networks ICTON '15," (2015).

1. Introduction

Gain saturation of pump degenerate four wave mixing (FWM) is often cited as a means of achieving all-optical amplitude regeneration of single amplitude level transmissions [1]. A reduction in amplitude noise in a signal may increase the transmission reach by two means. Firstly, it may constitute a real improvement in the signal to noise ratio of a transmission or potentially reshape the noise distribution to make it less harmful to the signal. Secondly, it may be seen as a preemptive measure against the generation of phase noise by preventing one of its major sources - amplitude noise to phase noise conversion from channel nonlinearities [2, 3].

The benefits of saturated FWM based methods over other approaches (such as nonlinear optical loop mirrors [4] and gain saturation in semiconductor optical amplifiers [5]) are in their relative simplicity as well as their possible dual use as amplifiers [6], wavelength converters [7] or even optical phase conjugators [8, 9]. Amplitude squeezing of a signal through saturated FWM is often described as occurring due to pump depletion. Such an explanation perhaps does not capture the richness of the underlying phenomenon, which may instead be viewed as depending upon the complicated interaction between the pump, the signal and the evolved harmonics as power flows between them during propagation.

Attempting to solve FWM of copropagating waves using coupled equations often results in the adoption of an undepletable pump approximation [10]. Such solutions are naturally of no use in understanding saturated FWM. By instead considering a single initial field consisting of multiple oscillating terms, an exact solution to FWM in the dispersionless case can be derived in which the evolution of harmonics as they propagate through the medium is descibed by the sum of two Bessel functions of differing order [10, 11]. In opting for this model, we cannot easily incorporate dispersion, which in general affects phase matching and FWM efficiency, however such effects are well understood and are studied in [3, 11, 12]. In this particular study we operate with high power ($\sim$1 W), short fibre length ($\sim$1 km), large nonlinearity ($\sim$10 $\mathrm{W^{-1}km^{-1}}$), low dispersion (D <0.4 $\mathrm{psnm^{-1}km^{-1}}$) and small channel spacing (40 GHz) and show that the model describes the experiment well, within this operating regime. These conditions are not inconvenient and are easily achieved. The model used enables us to explore the effect of pump to signal ratio upon unwanted phase noise, which is our main focus, but exact results may vary when dispersion is strong [3, 12].

We apply the Bessel function model of FWM [10, 11] to extract the conditions under which

amplitude squeezing of a signal can be achieved. Under these conditions, we derive expressions for the terms responsible for amplitude noise to phase noise conversion. Most importantly, by studying these terms we devise a means of suppressing this deleterious amplitude to phase noise conversion. To verify the method, we first experimentally confirm the validity of the Bessel function model of FWM in the saturation regime of our highly nolinear fibre setup, we then implement an amplitude regenerator, compare its behaviour with that predicted by theory and demonstrate phase preserving amplitude regeneration of a QPSK signal loaded with broadband amplitude noise. This paper extends preliminary results which were presented at CLEO 2015 [13].

2. Theoretical background and experimental verification

In this section, we provide a derivation of the FWM model used to determine the conditions for amplitude saturation and the sources of amplitude to phase noise conversion, providing experimental validation of the major results as appropriate. Supporting experimental data were collected by means of the setup shown in Fig. 1 which highlights one of the main features of saturated FWM based amplitude regeneration: its simplicity. A pump at 192.46 THz and a signal at 192.42 THz (shown in orange in Fig. 1) are coupled together using a 3 dB coupler and then gated with a 1/8 duty cycle using a Mach-Zehnder modulator (not shown in Fig. 1), resulting in rectangular pulses of 2 ns duration. The signal and pump then pass through a programmable filter (PF) which enables accurate control of their powers. The output of the PF is amplified using an erbium doped fibre amplifier (EDFA) before entering the nonlinear medium. Given the fixed power output of the EDFA used before the HNLF, gating the pump and signal, although having no appreciable effect upon the average output power of the EDFA, results in increased peak power of the pump and signal after amplification. For this study, it is desireable to have the facility to achieve a large value of $P\gamma L$ (the product of the pump power, nonlinear coefficient and medium length). The value of γ is determined by the nonlinear fibre technology available, and so the only way to increase γL is by increasing the length of HNLF. Unfortunately, increasing the length of the HNLF also decreases the Brillouin threshold at the same time [14]. To counteract this effect, we increase length by connecting a cascade of HNLFs to each other using optical isolators, which help to increase the Brillouin threshold [15]. The HNLF cascade used consisted of 0.5 km of 4 low dispersion HNLFs (dispersion, $|D| < 0.4\text{psnm}^{-1}\text{km}^{-1}$ and dispersion slope, $|D'| \leq 0.025\text{ps}^2\text{nm}^{-1}\text{km}^{-1}$) with mean nonlinear index γ_{mean} =9.7 $\text{W}^{-1}\text{km}^{-1}$ and effective length L_{eff} =0.149 km. The HNLFs used had a linear strain along their length, further increasing their Brillouin threshold [16], and the use of gated signals, whose bandwidth extends beyond the Brillouin gain bandwidth of the fibre, increases this threshold further. The output of the HNLFs (shown in the blue spectrum of Fig. 1) is analysed using an optical spectrum analyser (OSA).

In the following derivation, we mainly follow the approach presented by Mahric [11], although that presented by Lichtman et al [10] provides analogous results. First of all, we describe the pump and signal before undergoing FWM as two copropagating waves following $\Psi_0 = \sqrt{P_0}e^{i(\omega_0 t+\phi_0)}$ and $\Psi_1 = \sqrt{P_1}e^{i(\omega_1 t+\phi_1)}$, respectively, where P_m is the power of the wave, ω_m its radial frequency and ϕ_m its phase. Hence, m is defined such that the pump is denoted by $m = 0$ and the signal by $m = 1$. If they undergo FWM, the resultant field can be viewed to consist of a series of harmonics (as shown in blue in Fig. 1), which we shall label $\Psi'_m = \sqrt{P'_m}e^{i(\omega'_m t+\phi'_m)}$, where X' denotes the quantity X after it has propagated through the nonlinear medium. Starting from the nonlinear Schrödinger equation in the lossless and dispersionless case as a starting point:

$$\frac{\partial A(z,t)}{\partial z} = i\gamma|A(z,t)|^2 A(z,t) \tag{1}$$

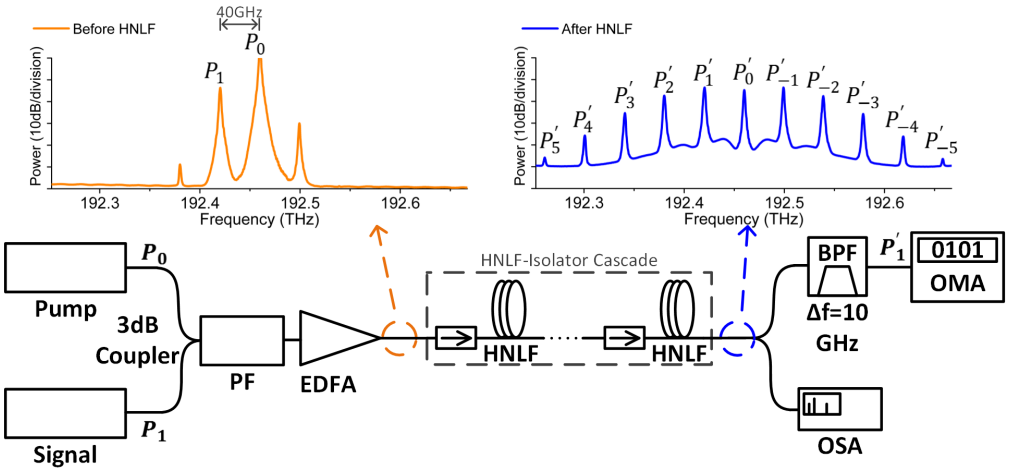

Fig. 1. Experimental setup used throughout this study. Inset figures show example spectrum before (orange) and after (blue) the HNLFs.

where $A(z,t)$ is the complex electric field amplitude. We justify the neglect of dispersion by noting that, for efficient FWM, the medium selected will likely have low net dispersion relative to its nonlinearity to ensure good phase matching, in other words, the nonlinear length should be much shorter than the dispersion length [17]. The inclusion of attenuation amounts to replacing the length of the medium by the effective length [10, 17]. Equation (1) may be solved directly to yield:

$$A(L,t) = A(0,t)e^{i\gamma|A(0,t)|^2 L} \tag{2}$$

If we substitute into this equation the sum of the two input waves, i.e. $A(0,t) = \Psi_0 + \Psi_1$, and expand the resulting equation, we may obtain the following:

$$A(L,t) = [\sqrt{P_0}e^{i(\omega_0 t+\phi_0)} + \sqrt{P_1}e^{i(\omega_1 t+\phi_1)}] \cdot e^{i\gamma L(P_0+P_1)} \cdot e^{2i\sqrt{P_0P_1}\gamma L\cos[(\omega_0-\omega_1)t+\phi_0-\phi_1]} \tag{3}$$

In order to recast this equation in terms of harmonics, we make use of the Jacobi-Anger expansion, $e^{ix\cos(\theta)} = \sum_{n=-\infty}^{\infty} i^n J_n(x)e^{in\theta}$, where $J_n(x)$ is the nth order Bessel function of the first kind. Grouping harmonics of the same order, we obtain the following:

$$A(L,t) = \sum_{m=-\infty}^{\infty} \sqrt{P'_m}e^{i(\omega'_m t+\phi'_m)} \tag{4}$$

where:

$$\begin{aligned}\sqrt{P'_m}e^{i(\omega'_m t+\phi'_m)} =& e^{i\gamma LP_0}e^{i\gamma LP_1} \\ & \left\{i^m\sqrt{P_0}J_m(2\sqrt{P_0P_1}\gamma L) + i^{m-1}\sqrt{P_1}J_{m-1}(2\sqrt{P_0P_1}\gamma L)\right\} \\ & \times e^{i[m(\omega_1 t+\phi_1)-(m-1)(\omega_0 t+\phi_0)]}\end{aligned} \tag{5}$$

where P'_m is the output power of the particular harmonic m. The power relationship for each harmonic may be obtained simply by taking the modulus squared of Eq. (5):

$$P'_m = P_0J_m^2(2\sqrt{P_0P_1}\gamma L) + P_1J_{m-1}^2(2\sqrt{P_0P_1}\gamma L) \tag{6}$$

where $J_n^2(x) := (J_n(x))^2$. Each harmonic can be seen to be described by two Bessel functions with identical arguments and of consecutive order, one proportional to the pump power and the other to the signal power.

To test the validity of the theory, we used the setup in Fig. 1, holding P_0 =7 W (38.4 dBm) and varying P_1 whilst measuring the output power of each harmonic, $\mathrm{P}'_{\mathrm{m}}(P_1)$, with $-6 \leq m \leq 6$. Figure 2 shows the results, experimental data being plotted with points and analytical curves with lines. The results for the first harmonic were fitted using Eq. (6) with $m = 1$ by varying the parameter γL and the result used to plot all other harmonics shown in Fig. 2 using the appropriate power relation obtained from Eq. (6). Very good agreement can be seen between the experimental data and these plots, however the accuracy of the fit falls off for higher signal input powers. This is likely due to the effect of dispersion not being considered in the theory [3, 12], effectively neglecting the impact of imperfect phase matching which is more noticeable at higher input signal power levels and for the pump ($m = 0$).

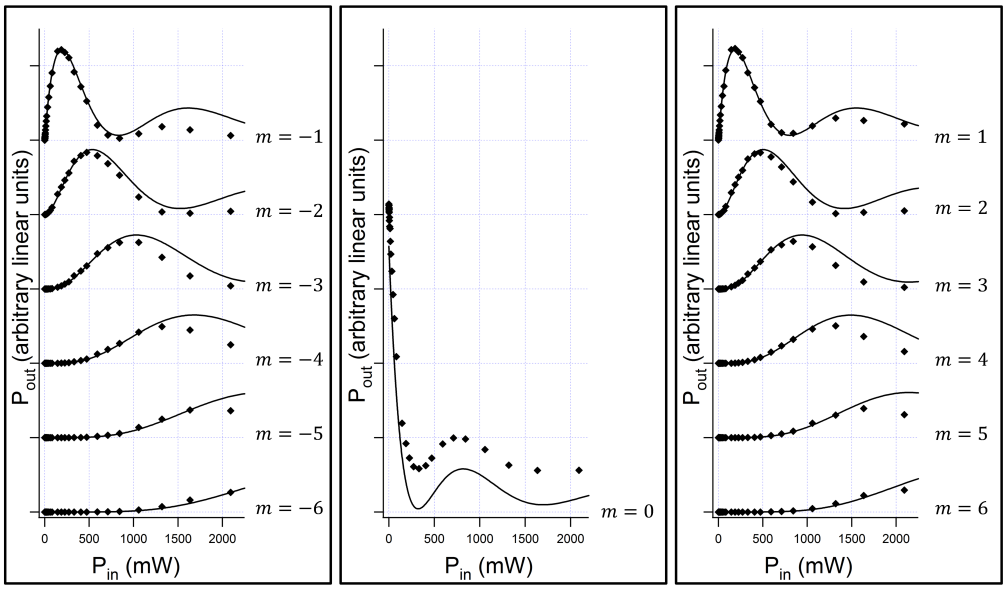

Fig. 2. Plots of output harmonic powers as they vary with signal input power for $-6 \leq m \leq 6$. Experimental data shown with points, analytical curves with lines.

Considering now the behaviour of the signal alone ($m = 1$), as it is the object of the amplitude regeneration, Eq. (5) becomes:

$$\sqrt{P_1'}e^{i(\omega_1' t+\phi_1')} = \underbrace{e^{i\gamma L P_0}}_{\text{XPM}}\underbrace{e^{i\gamma L P_1}}_{\text{SPM}}\underbrace{\left\{i\sqrt{P_0}J_1(2\sqrt{P_0P_1}\gamma L)+\sqrt{P_1}J_0(2\sqrt{P_0P_1}\gamma L)\right\}}_{\text{FWM Evolution}}\underbrace{e^{i(\omega_1 t+\phi_1)}}_{\text{Oscillatory Terms}} \qquad (7)$$

We obtain its power and phase relationships by taking the modulus square and complex argument, respectively, of Eq. (7), and identify potential sources of phase noise, cross-phase modulation (XPM), self-phase modulation (SPM) and Bessel-order mixing (BOM), to be discussed

later:

$$P_1' = P_0 J_1^2(2\sqrt{P_0 P_1}\gamma L) + P_1 J_0^2(2\sqrt{P_0 P_1}\gamma L) \tag{8}$$

$$\phi_1' = \phi_1 + \underbrace{\gamma L P_0}_{\text{XPM}} + \underbrace{\gamma L P_1}_{\text{SPM}} + \underbrace{\arctan\left\{\frac{\sqrt{P_0}J_1(2\sqrt{P_0 P_1}\gamma L)}{\sqrt{P_1}J_0(2\sqrt{P_0 P_1}\gamma L)}\right\}}_{\text{BOM}} \tag{9}$$

The term identified as XPM in Eq. (9) differs from the more commonly seen representation: $\mathbf{2}\gamma L P_0$. The extra factor of two would be obtained by expanding the term for BOM, and hence the full action of what would normally be considered XPM is incorporated within this term.

Using Eqs. (8) and (9), we may plot the curves in Fig. 3. The upper plot of Fig. 3 contains curves of the phase shift the signal experiences due to SPM and BOM, and shall be discussed later. The lower plot of Fig. 3 shows the first term (plotted in blue) and second term (plotted in pink) of Eq. (8), as well as the resultant signal power which occurs from their summation (plotted in black), for $\gamma L = 1\,\mathrm{W}^{-1}$ and $P_0 = 1\,\mathrm{W}$ (for illustrative purposes). As the input power of the signal, P_1, is increased, its output power, P_1' can also be seen to increase until it reaches a maximum, located at the dashed vertical line, after which it decreases. If we set (for instance, through use of an amplifier) the mean signal input power, $\langle P_1 \rangle$, such that it lies at this maximum, variations about the mean (shown by the grey vertical band) will be squeezed by the peak, resulting in much smaller variations of the output signal power, P_1' (shown by the grey horizontal band). This is in essence the underlying principle behind saturated FWM based amplitude squeezing. The first and second terms in Eq. (8) are proportional to P_0 and P_1, respectively, and so their relative contributions to the shape of P_1' plotted by the black line in Fig. 3 are determined by the pump to signal power ratio, $P_0 : P_1$. As both terms in Eq. (8) share the same argument, $x = 2\sqrt{P_0 P_1}\gamma L$, for a given $P_0 : P_1$ ratio, there is a value, $x = x_0$, such that P_1' is at its first maximum.

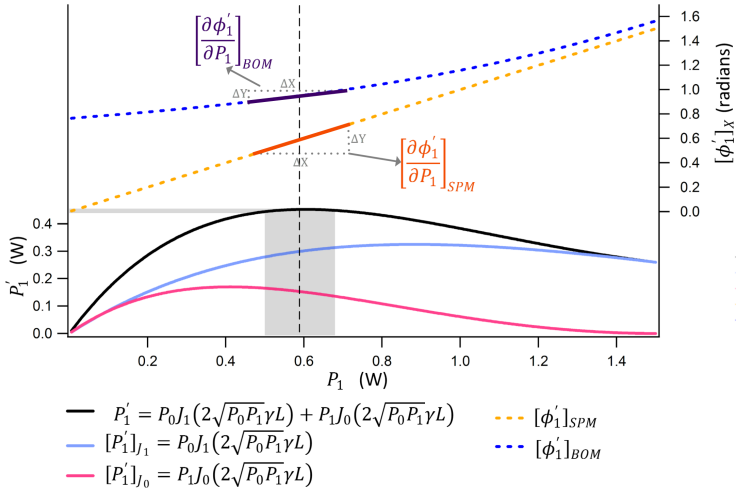

Fig. 3. Upper: Plots of SPM (orange dashed line) and BOM (blue dashed line) induced phase shift against P_1. Lower: Plot of P_1' (black solid line) and its summands, $J_0(x)$ and $J_1(x)$.

For high pump to signal power ratio, such that $P_0 \gg P_1$, Eq. (8) may be approximated by

only a single Bessel function:

$$P_1' \approx P_0 J_1^2(2\sqrt{P_0 P_1}\gamma L) \tag{10}$$

In this case, the operating point to achieve amplitude squeezing becomes the first peak of $J_1(x)$, which occurs at $x = x_0 = 1.84$.

Similarly, in the inverse case, where $P_1 \gg P_0$, Eq. (8) becomes dominated by its second term, leading to the following approximation:

$$P_1' \approx P_1 J_0^2(2\sqrt{P_0 P_1}\gamma L) \tag{11}$$

Which can be shown to have a maximum at $x = x_0 = 1.26$. Figure 4 shows a plot of x_0, true for all values of γL, as it varies with $P_0 : P_1$. Clearly visible are the two extreme cases where $x_0 = 1.26$ and $x_0 = 1.84$, as discussed above, as well as a smooth transition between these two values which occurs at intermediate $P_0 : P_1$ ratios.

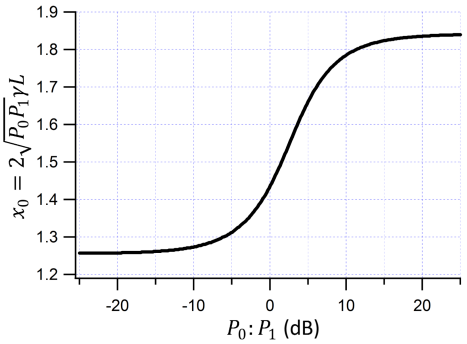

Fig. 4. Plot of the argument of the Bessel functions required to achieve amplitude squeezing (x_0) against pump to signal power ratio $P_0 : P_1$.

Dividing Eq. (8) by P_1 yields a relationship for the signal gain:

$$G = \frac{P_1'}{P_1} = \frac{P_0}{P_1} J_1^2(2\sqrt{P_0 P_1}\gamma L) + J_0^2(2\sqrt{P_0 P_1}\gamma L) \tag{12}$$

As is well known [11, 17], Eq. (12) shows that a greater signal gain may be achieved by increasing the pump to signal power ratio. For large enough $P_0 : P_1$, the argument of the Bessel functions at saturation will be $x_0 = 1.84$ and additionally, the first term in Eq. (12) will dominate the second, which may then be neglected. In this regime the gain experienced by the signal may be approximated as $G \approx (P_0/P_1) J_1^2(x_0) \approx P_0/3P_1$.

If so desired, we can obtain a relationship describing the distribution of power amongst the harmonics during saturation. In the high pump to signal power regime, Eq. (6) becomes $P_m' = P_0 J_m^2(2\sqrt{P_0 P_1}\gamma L) = P_0 J_m^2(x_0)$. Using this equation, we may obtain the harmonic to signal power ratio ($P_m' : P_1'$), which describes the power contained in each harmonic relative to the signal. Recalling that $x_0 = 1.84$ in the high saturation regime $P_m' : P_1'$ is given by:

$$\frac{P_m'}{P_1'} = \frac{J_m^2(x_0)}{J_1^2(x_0)} = \frac{J_m^2(1.84)}{0.34} \tag{13}$$

Following the same methodology, we can find $P'_m : P'_1$ for the low pump to signal power regime as well, where $x_0 = 1.26$:

$$\frac{P'_m}{P'_1} = \frac{J^2_{m-1}(x_0)}{J^2_0(x_0)} = \frac{J^2_{m-1}(1.26)}{0.41} \tag{14}$$

Using these relationships, it may be shown that the spectral extent is greater in the high pump to signal power case than the low pump to signal power case.

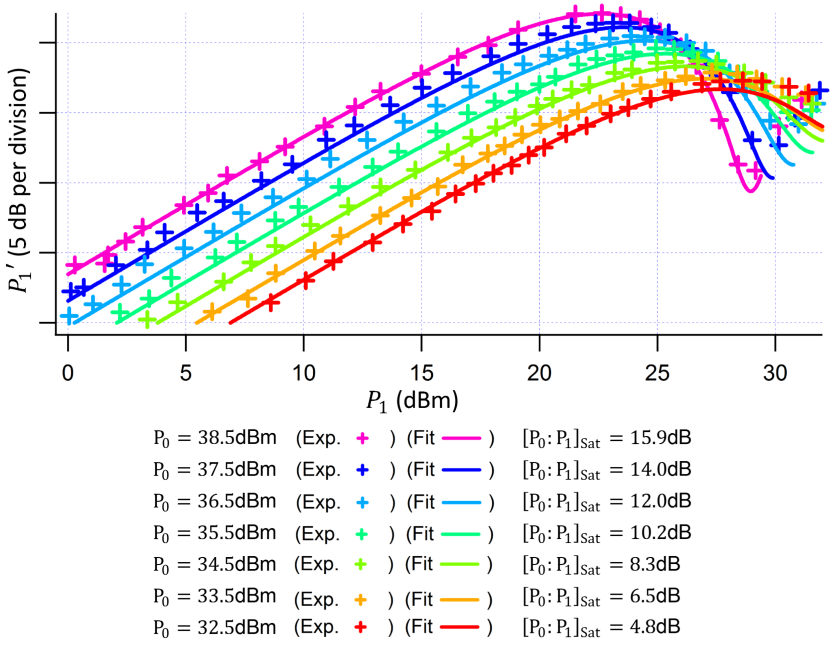

Fig. 5. Plots of the output signal power, P'_1 as it varies with input signal power, P_1 for different pump powers, P_0. Experimental data are plotted with crosses and analytical curves with lines.

Again, using the experimental setup in Fig. 1, we now map the function $\mathrm{P_1}'(P_1)$ for different values of P_0. Figure 5 shows the results of these measurements for seven different values of P_0, from 32.5 dBm to 38.4 dBm. The curves are plotted using the same estimate of γL as before. A very good match between experimental data and the theoretical plots can be seen for all of the cases. With increasing pump power, we see that not only does P'_1 peak for smaller values of P_1, but also the gain the signal experiences is larger, as predicted by Eq. (12).

We shall now consider sources of phase noise intrinsic to the system. Equation (9) contains four terms which contribute to the output phase of the signal. The first term, ϕ_1 is simply the input phase of the signal and carries with it the phase noise of the original signal, although it does not lead to any further increase in phase noise itself. The second term, $\gamma L P_0$ can be seen to represent the XPM the signal experiences from the pump. This source of phase noise is often neglected on the assumption that the pump used will possess such low amplitude noise that its contribution to the output phase noise of the signal is minimal. For now, we shall do the same but note that, as the impact of XPM increases with increasing pump power, pump power cannot be increased forever without consequence, which has been comprehensively studied in [18, 19].

The third term in Eq. (9), $\gamma L P_1$ embodies the SPM the signal induces upon itself and, due to its dependence upon P_1, it constitutes a source of amplitude noise to phase noise conversion. The final term, $\arctan\left\{\sqrt{P_0}J_1(2\sqrt{P_0P_1}\gamma L)/\sqrt{P_1}J_0(2\sqrt{P_0P_1}\gamma L)\right\}$ is a consequence of the fact that the Bessel functions describing the harmonic evolution are orthogonal but vary in power, resulting in a variation of phase. We refer to this term as Bessel-order mixing, BOM [13].

The top plots in Fig. 3 show the phase shift of the output signal, ϕ_1', due to SPM (plotted in orange) and BOM (plotted in blue). We note that absolute phase shifts themselves do not constitute phase noise, and it is really the change in output signal phase with input signal power, $\frac{\partial\phi_1'}{\partial P_1}$, which results in amplitude noise to phase noise conversion. We operate at the peak of the black power curve in Fig. 3, identified by the dashed black line, and so it is the derivatives of the phase curves about the peak, as shown in Fig. 3 which are responsible for phase noise generation.

The variance of ϕ_1', $\sigma^2_{\phi_1'}$ due to power fluctuations may be approximated to first order by:

$$\sigma^2_{\phi_1'} = \left(\frac{\partial\phi_1'}{\partial P_1}\right)^2 \sigma^2_{P_1} \tag{15}$$

where $\sigma^2_{P_1}$ is the variance of the signal input power, P_1. If we amplify a signal with an ideal amplifier, its variance will change but its fractional variation will not. Hence fractional variation, $\varepsilon_{P_1} = \sigma_{P_1}/\langle P_1\rangle$, also known as the coefficient of variance, is a more useful metric in this instance and is adopted here. Equation (15) then becomes:

$$\sigma^2_{\phi_1'} = \left(\langle P_1\rangle \frac{\partial\phi_1'}{\partial P_1}\right)^2 \varepsilon^2_{P_1} = \Gamma^2\varepsilon^2_{P_1} \tag{16}$$

Hence, the factor $\Gamma = \langle P_1\rangle \frac{\partial\phi_1'}{\partial P_1}$ directly represents the severity of amplitude noise to phase noise conversion. To obtain a value for Γ, we take the derivative of Eq. (9) with respect to P_1 and multiply the result by $\langle P_1\rangle$:

$$\Gamma = \langle P_1\rangle \frac{\partial\phi_1'}{\partial P_1} = \underbrace{\langle P_1\rangle \gamma L}_{\Gamma_{\mathrm{SPM}}} + \underbrace{\langle P_1\rangle \frac{\partial}{\partial P_1}\arctan\left\{\frac{\sqrt{P_0}J_1(2\sqrt{P_0P_1}\gamma L)}{\sqrt{P_1}J_0(2\sqrt{P_0P_1}\gamma L)}\right\}}_{\Gamma_{\mathrm{BOM}}} \tag{17}$$

where we have left the final derivative unresolved due to its complicated mathematical representation. Figure 6 provides plots for the two amplitude to phase noise terms identified in Eq. (17), Γ_{SPM} (orange) and Γ_{BOM} (blue) when operating at x_0 (saturation) as they vary with pump to signal power ratio, both with a linear scale (plot a)) and a logarithmic scale (plot b)). These plots are valid for all values of γL and show that the degree of phase preservation depends only upon the pump to signal power ratio. Focusing first upon the linear plot in Fig. 6(a), we see that the effect of SPM diminishes for increasing $P_0 : P_1$. This makes sense, as the SPM term follows $\Gamma_{\mathrm{SPM}} = \langle P_1\rangle \gamma L$ and for a given $P_0 : P_1$ at saturation, $x_0 = 2\sqrt{P_0\langle P_1\rangle}\,\gamma L$ is true, therefore $\Gamma_{\mathrm{SPM}} = 2\sqrt{\langle P_1\rangle/P_0}\,x_0$, which is inversely proportional to the square root of $P_0 : P_1$. Γ_{BOM}, on the other hand shows a peak around 4 dB and reduces either with increasing or decreasing $P_0 : P_1$. This time, inspection of Eq. (7) reveals the cause of this behaviour. BOM can be seen to be the result of the interaction between the two orthogonal Bessel terms. If either P_0 or P_1 becomes overwhelmingly larger than the other, it will dominate the phase of the output signal making the variation of phase because of the other term negligible. When the two terms are comparable we observe a maximum of phase variation, hence the peak at $P_0 : P_1$=4 dB.

The logarithmic plots of Fig. 6 assist comparison of the relative importance of SPM and BOM. Γ_{SPM} can be seen to decrease monotonically with increasing $P_0 : P_1$, with a small deviation about $P_0 : P_1$=4 dB, which corresponds to the transition region of x_0 shown in Fig. 4.

Γ_{SPM} is larger than Γ_{BOM} for all values of $P_0 : P_1$. For $P_1 \gg P_0$, Γ_{SPM} renders the effect of Γ_{BOM} negligible and is the major cause of amplitude noise to phase noise conversion. However, at the other extreme, with $P_0 \gg P_1$ $\Gamma_{\mathrm{BOM}}/\Gamma_{\mathrm{SPM}}$ tends towards a constant value of approximately 0.7, i.e. although $\Gamma_{\mathrm{BOM}} < \Gamma_{\mathrm{SPM}}$, Γ_{BOM} is responsible for about 40% of the total amplitude to phase noise conversion, Γ, at high $P_0 : P_1$ levels.

As the pump to signal power ratio is increased, the severity of XPM increases whilst that of SPM decreases, implying that there is a trade-off between SPM and XPM [18, 19]. Matsumoto et al [18] found through simulation, that even for $P_0 : P_1$ as high as 36 dB at saturation, a pump OSNR of 50 dB results in a negligible impact on the phase noise of the squeezed output. Given that the OSNR of the lasers used as pumps in this study are in excess of 50 dB and the highest $P_0 : P_1$ for which saturation is achieved using data is 13 dB (as the demonstration of larger ratios is denied by the onset of Brillouin scattering), XPM should not be an issue for the present study and will be ignored. Further theoretical analysis of the trade-off between XPM and SPM has been presented in [19]. Later in this paper, it will be shown experimentally that the quality of the pump used, being of low RIN (as typically used in FWM experiments), is such that XPM does not play a major role in the experiments and so we are free to neglect its effect in this analysis.

The conclusion, shown clearly by either plot in Fig. 6 is this: for this specific scheme, although saturation can be achieved, in theory, for any value of $P_0 : P_1$, amplitude noise to phase noise conversion from all sources is determined only by $P_0 : P_1$ and may only be reduced by pursuing a high $P_0 : P_1$ ratio. Given that saturation occurs at $x_0 = 2\sqrt{P_0 P_1}\gamma L$, pursuing as large a value of $P_0 : P_1$ as possible implies the need to increase P_0, γ and/or L whilst simultaneously decreasing P_1 to maintain the equality. In practical implementations, the magnitude of γL will be limited by the technology available and similarly the maximum usable pump power is often restricted to prevent damage to devices or adverse effects such as Brillouin scattering and/or two photon absorption. Such factors mean that real world implementations of amplitude regenerators based on saturated FWM often make use of signal powers comparable to the pump power. We note that, by increasing pump to signal power ratio through the use of an increased pump power and reduced signal power, not only can we eliminate SPM and BOM, but we can also extract a much greater signal gain from the system - something which is sacrificed when a low pump to signal ratio is used.

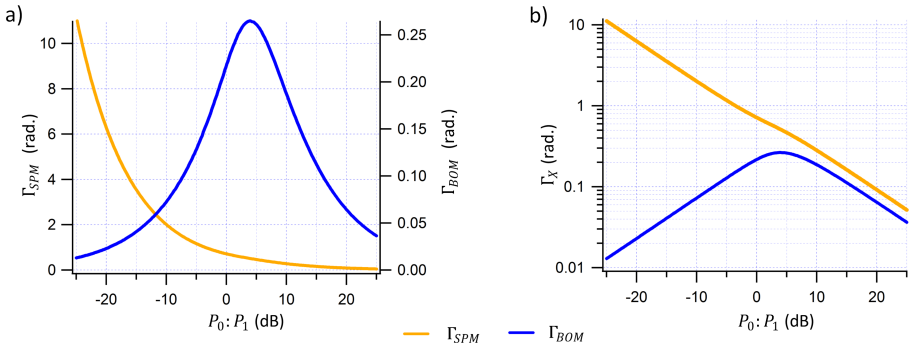

Fig. 6. a) linear and b) logarithmic plots of Γ_{SPM} (orange) and Γ_{BOM} (blue) as they vary with pump to signal power ratio $P_0 : P_1$ at peak.

3. Performance as an amplitude regenerator

Following the conclusions of the previous sections, we now proceed to demonstrate the benefits of high pump to signal power ratio by performing amplitude regeneration upon QPSK signals.

For this demonstration, the setup in Fig. 1 was modified by removing the gating (rendering the pump CW) and replacing the signal with a 10 Gbaud, non-return-to-zero QPSK signal carrying two quadrature multiplexed PRBS-15 data streams. QPSK is a data format which, whilst being quite robust against amplitude noise, is much more sensitive to phase noise, making it ideal for gauging phase preservation. The use of a CW pump reduces the maximum pump power that can be used due to SBS. To overcome this, the fibre cascade was reconfigured, resulting in an additional 1 km of fibre being added. It should be noted, therefore, that the pump powers in the previous study using a gated pump and signal may not be directly compared to those used in the following section. To contaminate only the signal's amplitude with broadband noise, the signal passes through an appropriately biased Mach-Zehnder modulator which is driven by the electrically amplified output of a fast photodiode exposed to ASE. To extract the signal after amplitude squeezing, we use an optical band pass filter and then measure the signal using an optical modulation analyser (OMA). We characterise the regenerator for several different pump powers, each time optimising the mean signal power to achieve saturation.

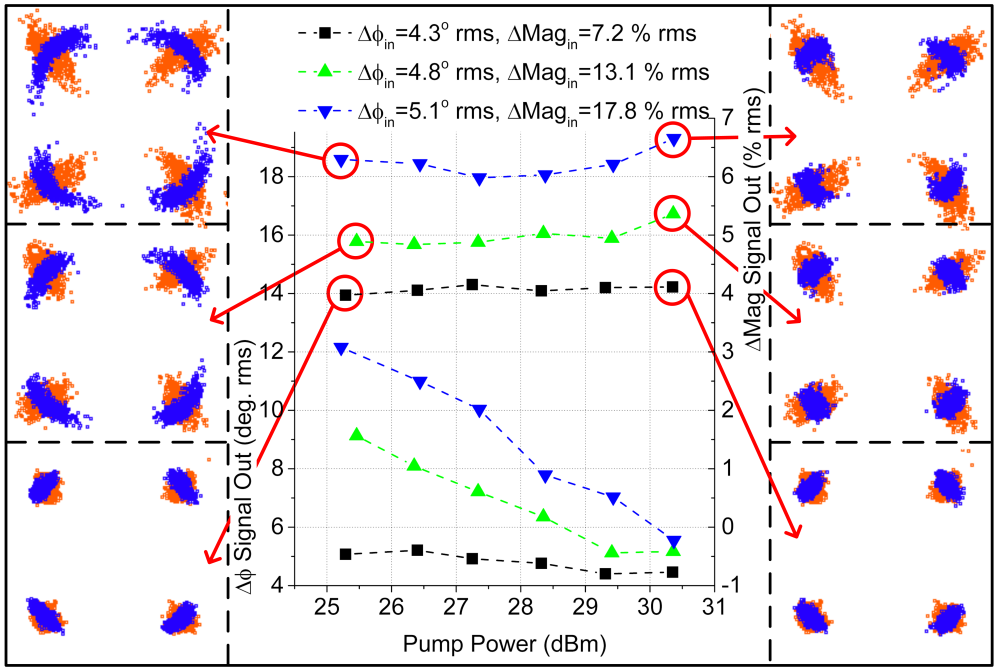

Fig. 7. Central graph provides output phase and amplitude noise statistics for 3 input amplitude noise levels as they vary with pump power. Constellation plots on the left and right correspond to the lowest and highest pump powers used, respectively.

Figure 7 provides the output phase noise, $\Delta\phi'_m$ (lower left axis), and amplitude noise, ΔMag (upper right axis) statistics as they vary with the pump power of the system for three different input amplitude noise cases. Constellation plots are provided for these noise scenarios for both the lowest pump power system and the highest pump power system. Focusing on the noise statistics first of all, we see that the output amplitude noise of the system varies little with pump power, in other words, changing the $P_0 : P_1$ ratio does not compromise the ability of the

regenerator to correct amplitude noise. We note that, even with no extra amplitude noise added to the signal, which results in ΔMag =7.2 %rms, the amplitude noise is improved in all cases to approximately 4 %rms. Output amplitude noise, however, does depend upon input noise, and this is because the amplitude squeezing region of the power transfer curve is a peak and not a plateau, as shown in Fig. 5.

Output phase noise depends heavily upon the input amplitude noise as well as on the selected pump power. For the lowest input noise case, that of ΔMag =7.2 %rms, output phase noise is almost flat with pump power and is very similar in magnitude to the 4.3 deg rms phase noise of the input, showing that all of the regenerators impart little amplitude-independent phase noise. This result also supports our decision to disregard phase noise due to XPM; as pump power is increased, there is no increase in output signal phase noise (in fact, it decreases).

For the two higher input amplitude noise levels, ΔMag =13.1 %rms and ΔMag =17.8 %rms, we see that phase noise decreases drastically with increasing pump power. For ΔMag =17.8 %rms, using the lowest pump power of 25.3 dBm results in an increase in phase noise due to regeneration from 5.1 deg rms to 12.1 deg rms, an increase of 130%. In contrast, using the highest pump power, 30.3 dBm, results in an almost negligible increase in phase noise of only 0.8%, proving the effectiveness of using high pump power to achieve phase preservation.

The constellation plots echo these results and show that, although for the lowest input amplitude noise there is very little increase in phase noise through regeneration regardless of the pump power used, for the highest input amplitude noise in the low pump power case we see an increase in phase noise to the extent at which the amplitude regenerator is effectively useless, whilst for the high pump power case we have drastically reduced amplitude noise whilst suffering barely any increase in phase noise.

Finally, we consider how the regenerative ability of the system depends upon pump power in terms of receiver sensitivity. Figure 8 provides bit error ratio (BER) plots for the same 3 input amplitude noise levels considered above. We plot the BER for the unregenerated, noise loaded signal along with the results from using the highest pump power as well as the lowest pump power as it varies with the OSNR of the signal. For the lowest noise case, ΔMag = 7.2% rms, Fig. 8(a), we see, in agreement with the noise statistics and constellation plots above, that regeneration deteriorates the signal slightly, by about 0.5 dB, regardless of the pump power. In the middle noise case, corresponding to an input noise of ΔMag = 13.1% rms, we see that the low pump power regenerator still results in a power penalty to the signal after regeneration, meanwhile the high pump power case results in an improvement in receiver sensitivity of about 1 dB for a BER of 10^{-4}. In the highest noise case, with ΔMag = 17.8% rms, we see that regeneration with low pump power severely deteriorates the signal, even resulting in an error floor, whilst the high pump power case still results in an improvement in receiver sensitivity of 1.4 dB for a BER of 10^{-4}. Given the sensitivity of QPSK to phase noise, the improvement in receiver sensitivity upon regeneration can be seen as a testament to the magnitude of phase preservation achieved.

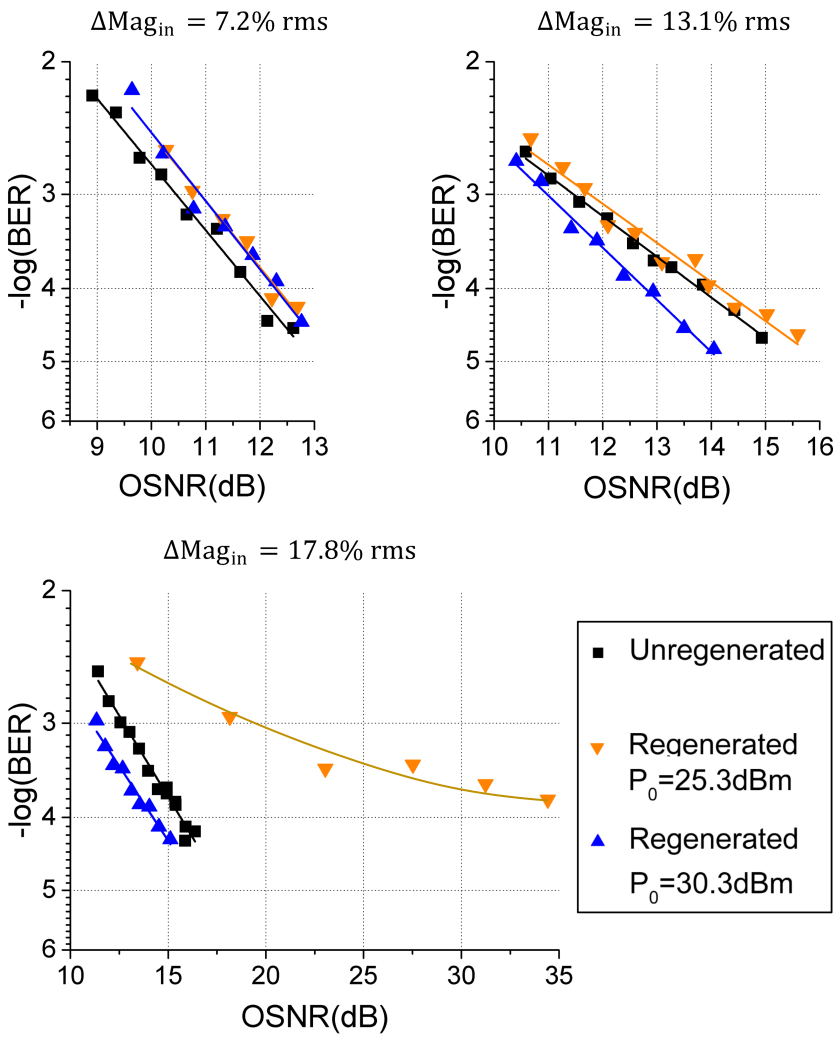

Fig. 8. Bit error ratio measurements for 3 input amplitude noise level cases.

4. Conclusion

The objective of this study was to understand and eliminate the underlying mechanisms behind amplitude noise to phase noise conversion in saturated FWM based amplitude regenerators. By making use of an exact solution to the nonlinear Schrödinger equation in the dispersionless case [10, 11], we presented the conditions required for amplitude saturation of a signal and determined the causes of amplitude noise to phase noise conversion during amplitude squeezing: SPM and BOM. We noted that the only way to eliminate both of these sources of phase noise is by increasing the pump to signal power ratio and doing so brings with it the added benefit of improved signal gain. In light of this understanding, we demonstrated phase preserving amplitude regeneration upon a 10 GBaud QPSK signal. We showed that regeneration of the signal using a pump to signal power ratio that is too low, for instance 4 dB, results in an intolerable degradation in the signal quality due to phase noise. In comparison, adoption of a higher pump to signal ratio of 13 dB, allows accrued phase noise to be reduced by a factor of 16.

Acknowledgments

This research is sponsored by EPSRC grant EP/I01196X, The Photonics Hyperhighway. Dr F. Parmigiani is supported by a Royal Academy of Engineering/EPSRC research fellowship. Dr G. Hesketh is supported by the EPSRC grant EP/M50662X/1. The data for this work is accessible through the University of Southampton Institutional Research Repository (DOI:10.5258/SOTON/386447).